J Solid State Electrochem (2012) 16:785–793
DOI 10.1007/s10008-011-1427-3

ORIGINAL PAPER

Oxygen excess nonstoichiometry and thermodynamic quantities of $La_2NiO_{4+\delta}$

S.-Y. Jeon · M.-B. Choi · J.-H. Hwang · E. D. Wachsman · Sun-Ju Song

Received: 7 April 2011 / Revised: 28 April 2011 / Accepted: 30 April 2011 / Published online: 20 May 2011

Abstract The oxygen excess nonstoichiometry of $La_2NiO_{4+\delta}$ is measured as a function of temperature and oxygen partial pressure (pO_2) by coulometric titration method. A positive deviation from the ideal dilution solution behavior is exhibited, and the partial molar thermodynamic quantities of $La_2NiO_{4+\delta}$ are calculated from the Gibbs–Helmholtz equation for regular solution by introducing the activity coefficient of the charge carriers. The activity coefficient of holes is successfully calculated by using the Joyce–Dixon approximation of the Fermi–Dirac integral. The effective mass of holes (m_h^*) is 1.27–1.29 times the rest mass (m_h), which indicate the action of band-like conduction and allow the effect of the small degree of polaron hopping to be ignored. The activity coefficient of holes calculated against the oxygen nonstoichiometry clearly illustrates the early positive deviation of the activity coefficient of holes from unit, leading to $\gamma_{h^\bullet} \approx 14$ at $\delta \approx 0.08$, which is quite close to the literature value of $\gamma_{h^\bullet} \approx 10$ at $\delta \approx 0.08$. All the evaluated thermodynamic quantities are in good agreement with the experimental literature values.

S.-Y. Jeon · M.-B. Choi · S.-J. Song (✉)
Department of Materials Science and Engineering,
Chonnam National University,
300 Yongbong-dong, Buk-gu,
Gwangju 500-757, South Korea
e-mail: song@chonnam.ac.kr

J.-H. Hwang
Department of Materials Science and Engineering,
Hongik University,
Seoul 121-791, South Korea

E. D. Wachsman
Department of Materials Science and Engineering,
University of Maryland,
College Park, MD 20742, USA

Keywords Oxygen nonstoichiometry · Activity coefficient · Hole degeneracy

Introduction

Due to the relatively high oxygen ion conductivity, p-type electronic conductivities, substantially high oxygen permeability, similar thermal expansion coefficient with yttrium-stabilized zirconia (YSZ), and low chemical expansion, undoped $La_2NiO_{4+\delta}$ has attracted significant attention for use in electrochemical devices such as cathodes of intermediate temperature solid oxide fuel cells, oxygen separation membranes, and electrocatalysts [1–4]. Numerous experimental results have shown that the dominant charge carriers are oxygen interstitials and electron holes in the relatively high oxygen hyperstoichiometric undoped $La_2NiO_{4+\delta}$ system [5–7]. Initially, the high oxygen ion conductivity of $La_2NiO_{4+\delta}$ has been elucidated from its crystal structure, consisting of alternating layers of rock salt LaO and perovskite $LaNiO_3$, which helps excess interstitial oxygen ions sitting at the center of the La tetrahedron migrate easily through the *a–b* plane of rack salt layer, while the contribution from the oxygen vacancies in the perovskite layer is very low [8, 9]. However, recent reports base on molecular dynamics calculation suggest an oxygen interstitialcy mechanism rather than the simple anion jumps between the interstitial positions [10–12].

Recently, an unusual positive deviation from the ideal dilute solution behavior has been identified by the monotonic increase of both oxygen excess nonstoichiometry and isothermal equilibrium conductivity with decreasing power to the oxygen activity in the N_2/O_2 regime, and these findings have been investigated for elucidating the electrical properties of $La_2NiO_{4+\delta}$ [13–15]. Especially, both the delocalized electron model with metallic band conduction and the small polaron model with localized electron migration have been reported as major p-type electrical conduction mechanisms [16, 17]. Furthermore, the $a_{O_2} - T - \delta$ diagrams were successfully described using a statistical thermodynamic approach that related the strongly non-ideal behavior to the coulombic repulsion of oxygen interstitials and the interaction of holes localized on the B-site cation [18]. On the other hand, a delocalized p-type metallic electron model was suggested from the behavior of the d_{x2-y2} electron in occupying a narrow σ_{x2-y2} band as an itinerant electron [19]. Further analysis of the positive deviation of electronic conductivity and thermoelectric power with respect to oxygen partial pressure (pO_2) in the N_2/O_2 regime was best fitted with a metallic conduction model by introducing the activity coefficients of both oxygen interstitials and holes, rather than the loss of charge carrier concentrations [16].

In this work, therefore, we analyze the unusual positive deviation of oxygen excess nonstoichiometry of $La_2NiO_{4+\delta}$ on the basis of the delocalized electron model and extract its thermodynamic properties by both solving the Gibbs–Helmholtz equation [16] and calculating the activity coefficient of the charge carriers by using the Joyce–Dixon approximation of the Fermi–Dirac integral from the partition function in the quasi-free-particle approximation with the regular solution model [15]. The extent of the oxygen excess nonstoichiometry of $La_2NiO_{4+\delta}$, i.e., δ, is measured by coulometric titration method as functions of the temperature ($1{,}073 \leq T/K \leq 1{,}273$) and pO_2 ($-14 \leq \log [pO_2/\text{atm}] \leq -1$). Finally, we compare the thermodynamic quantities calculated from the two different methods with the same delocalized p-type metallic band conduction model.

Experimental

Undoped $La_2NiO_{4+\delta}$ powders were prepared from the starting materials of lanthanum acetate hydrate ($C_6H_9LaO_6 \cdot H_2O$, 99.9%, Aldrich, USA) and nickel acetate tetrahydrate ($(C_2H_3O_2)_2Ni \cdot 4H_2O$, 99.9%, Aldrich, USA) by coprecipitation method. Stoichiometric amounts of each component were dissolved in distilled water and mixed together. Subsequently, a small amount of ammonium hydroxide was added to the system to adjust the pH to 10. The solution was dried under stirring condition and calcined at 1,173 K for 10 h in air. The calcined powder was then planetary ball-milled with stabilized zirconia balls six times for 0.5 h at 350 rpm, cold isostatically pressed at 150 MPa, and sintered at 1,623 K for 10 h in air.

The obtained powders were characterized by X-ray diffraction (D/MAX Ultima III, Rigaku, Japan) equipped with a Cu target X-ray tube at a scan rate of 1°/min between scanning angles of 2theta (10° and 90°). The X-ray spectra showed a single phase of orthorhombic $La_2NiO_{4+\delta}$ structure, as shown in Fig. 1a. The primary particle size of the calcined powders, d, was estimated from the X-ray line width by the Scherrer formula, $d = 0.9\lambda/\beta 1/2\cos\theta$, where λ is the X-ray wavelength, $\beta 1/2$ the corrected width of the main diffraction peak at half-height, and θ the diffraction angle. The d values of the powders were slightly less than 1 µm, which was close to the value calculated from the scanning electron micrograph (Shimadzu, SS-550) image of powders shown in Fig. 1b.

Coulometric titration cells were constructed as schematically shown in Fig. 2. As a solid electrolyte (1 in the figure), a disk of 8 mol% Y_2O_3-ZrO_2 solid solution (8 yttrium-stabilized zirconia), 12.5 mm diameter×1.0 mm thick, was polished on both planar surfaces with assorted diamond pastes of grit size down to 1 µm. As a gas electrode (8 in the figure), a piece of Pt gauze (29809-3, 100 mesh, Aldrich), measuring 2.5×2.5 mm, was subsequently attached to each polished surface of the YSZ disk with the aid of Pt paste (5542, unfluxed, Engelhard) by firing overnight at about 1,273 K in air atmosphere. Two alumina tubes (2 and 3 in the figure) served as a chamber to transfer a $La_2NiO_{4+\delta}$ specimen (7 in the figure) inside, and the empty space between the alumina tubes and the alumina cup (5 in the figure) was filled with silicate glass powder (6 in the figure) of composition 49 wt.% SiO_2, 25 wt.% BaO, 16 wt.% B_2O_3, and 10 wt.% Al_2O_3. At elevated temperatures, the glass powder melted to provide a satisfactory gas-tight seal [20, 21].

The oxygen nonstoichiometry (δ) of $La_2NiO_{4+\delta}$ was measured by a coulometric titration technique from a titration cell with the configuration shown in Fig. 2,

$$\text{Pt}, a_{O_2}|La_2NiO_{4+\delta}|\text{YSZ}\left|a_{O_2}^{\text{ref}}, \text{Pt}\right. \tag{1}$$

as detailed elsewhere. Briefly, a nonstoichiometric change, $\Delta\delta$, from a reference value δ^* at a starting oxygen activity a_{O_2} to the value d at another equilibrium a_{O_2} is determined as

$$\Delta\delta = \delta - \delta^* = \frac{It}{2F}\frac{M}{m_O} \tag{2}$$

and the final equilibrium oxygen activity as

$$a_{O_2} = a_{O_2}^{\text{ref}} \exp\left(\frac{4FE}{RT}\right) \tag{3}$$

Here, I denotes a constant current passed through the cell for a prefixed time duration t, M the molar weight of $La_2NiO_{4+\delta}$, m_o the initial mass of the specimen, E the open-circuit voltage across the YSZ after the specimen has been re-equilibrated, and $a_{O_2}^{\text{ref}}$ the oxygen activity of the reference gas flowing outside the titration cell. In the present

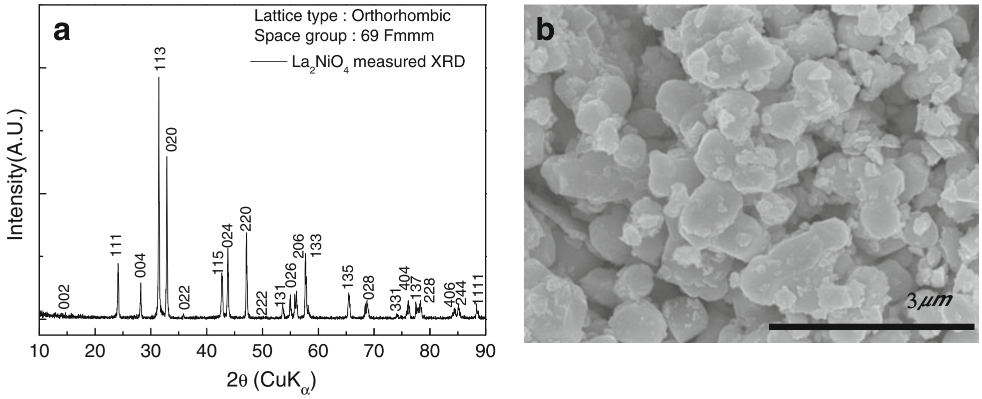

Fig. 1 **a** Room temperature X-ray diffraction patterns of $La_2NiO_{4+\delta}$ sintered at 1,623 K in air and **b** scanning electron micrograph of powders of $La_2NiO_{4+\delta}$ calcined at 1,273 K in air

experiments, N_2/O_2 or CO/CO_2 mixtures were employed as the reference gas to minimize the oxygen activity gradient across the YSZ. The nonstoichiometry was measured down to the oxygen activity where the system decomposes at three different temperatures, 1,073, 1,173, and 1,273 K. For the leak test, the pO_2 inside the cell was measured according to time after the abrupt change of pO_2 outside the cell while a constant pO_2 was maintained, as shown in Fig. 3. The absolute value for the nonstoichiometry was determined by gravimetric measurement of the overall mass loss upon decomposition via the reaction

$$La_2NiO_{4+\delta} \rightarrow La_2O_3 + Ni + \frac{1+\delta}{2} O_2(g) \tag{4}$$

as has been confirmed experimentally elsewhere [13, 15, 17, 22].

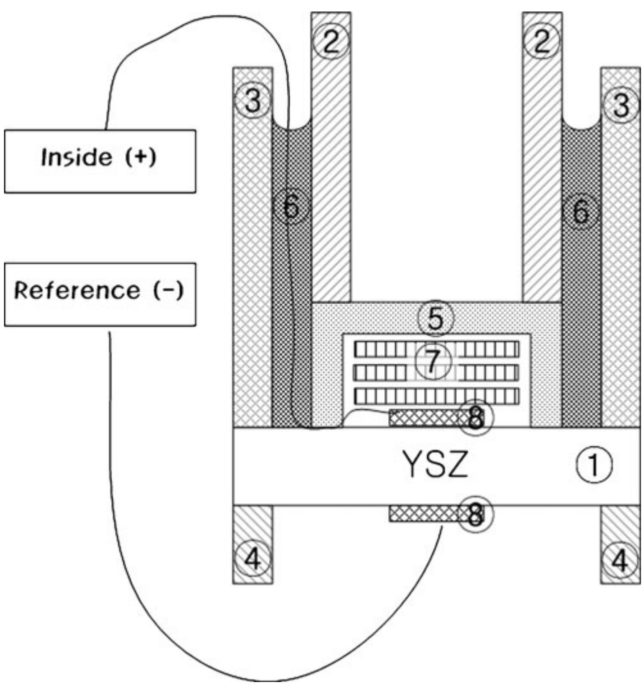

Fig. 2 Schematic of the as-constructed titration cell: *1* YSZ electrolyte, *2–4* alumina tubes, *5* impermeable alumina cup, *6* Pyrex glass, *7* specimen, *8* reversible electrode

Results and discussion

The nonstoichiometric oxygen contents of $La_2NiO_{4+\delta}$ at three different temperatures are shown in Fig. 4. The continuous nature of the isothermal nonstoichiometry, i.e., δ, indicated that our measurement was performed for the single phase of $La_2NiO_{4+\delta}$. Our nonstoichiometry, δ, measured by coulometric titration was in good agreement with the literature data and ranged from approximately 0 to ca. 0.10. The δ values increased with increasing temperature and with increasing a_{O_2} with ever decreasing power to the oxygen activity. The relationship of log δ vs. log a_{O_2}, as shown in the small inset of Fig. 4, can be divided into two regions. Below $a_{O_2} \leq 10^{-6}$ atm, the oxygen exponent at isothermal condition, $\delta \propto a_{O_2}^m$, shows m=1/6 as oxygen activity decreases, which is expected from the equilibrium defect diagram where oxygen interstitials and holes are considered as dominant defect species with the ideal solution model. Above $a_{O_2} \geq 10^{-6}$ atm, the oxygen exponent m decreases with increasing oxygen activity, suggesting the positive deviation of the system [13, 15].

The partial molar thermodynamic quantities of $La_2NiO_{4+\delta}$ may be calculated from the temperature dependence of

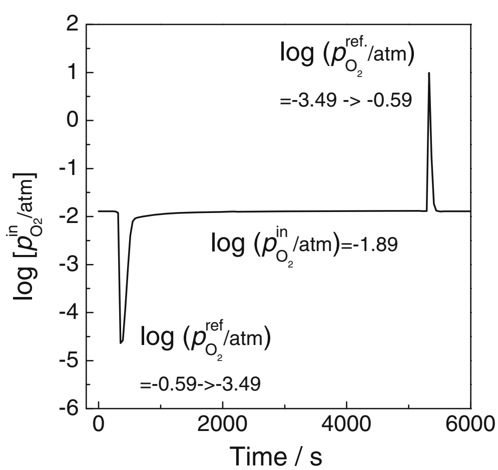

Fig. 3 Oxygen partial pressure (pO_2) change of the titration cell according to time during the leak test

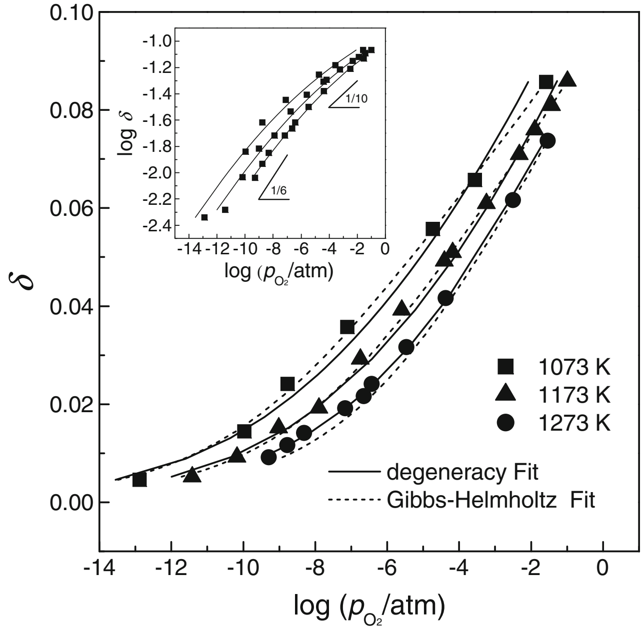

Fig. 4 Oxygen nonstoichiometry of δ vs. oxygen activity of $La_2NiO_{4+\delta}$ at various temperatures. *Inset*, both axes in logarithmic scale with an ideal slope of m=1/6. *Solid lines* are best fitted to hole degeneracy considering the Joyce–Dixon approximation of the Fermi–Dirac integral, and *solid broken lines* are best fitted to the Gibbs–Helmholtz equation for regular solution

oxygen nonstoichiometry by solving the Gibbs–Helmholtz equation. The molar Gibbs free energies for the mixing of oxygen relative to gaseous oxygen at the standard state, $\Delta\overline{G}_{\mathrm{O}}^{\mathrm{M}}$, is often expressed as a chemical potential difference:

$$\Delta\overline{G}_{\mathrm{O}}^{\mathrm{M}} = \mu_{\mathrm{O}} - \frac{1}{2}\mu_{\mathrm{O}_2}^{\mathrm{o}}(g) = \frac{RT}{2}\ln a_{\mathrm{O}_2}$$
$$= \left(\mathrm{h_O} - \frac{1}{2}\mathrm{h}_{\mathrm{O}_2}^{\mathrm{o}}\right) - T\left(\mathrm{s_O} - \frac{1}{2}\mathrm{s}_{\mathrm{O}_2}^{\mathrm{o}}\right) \tag{5}$$

where $\mu_{\mathrm{O}}^{\mathrm{o}}$ denotes μ_{O} in equilibrium with 1 bar oxygen. In addition, $h_{\mathrm{O}} - h_{\mathrm{O}}^{\mathrm{o}}$ is the partial molar enthalpy for the mixing of oxygen and $s_{\mathrm{O}} - s_{\mathrm{O}}^{\mathrm{o}}$ is the partial molar entropy for the mixing of oxygen, which may be calculated from:

$$\Delta\overline{H}_{\mathrm{O}}^{\mathrm{M}} = \mathrm{h_O} - \frac{1}{2}\mathrm{h}_{\mathrm{O}_2}^{\mathrm{o}} = \frac{\partial}{\partial(1/\mathrm{T})}\left(\frac{\mathrm{R}}{2}\ln \mathrm{a}_{\mathrm{O}_2}\right) \tag{6}$$

$$\Delta\overline{S}_{\mathrm{O}}^{\mathrm{M}} = s_{\mathrm{O}} - \frac{1}{2}s_{\mathrm{O}_2}^{\mathrm{o}} = \frac{\partial}{\partial T}\left(\frac{RT}{2}\ln a_{\mathrm{O}_2}\right) \tag{7}$$

Both $h_{\mathrm{O}} - h_{\mathrm{O}}^{\mathrm{o}}$ and $s_{\mathrm{O}} - s_{\mathrm{O}}^{\mathrm{o}}$ may be obtained from the slope of $R/2\cdot\ln a_{\mathrm{O}_2}$ vs. $1/T$ plot and $RT\cdot\ln a_{\mathrm{O}_2}$ vs. T plot for selected δ, as shown in Fig. 5. The values of the partial molar enthalpy and of the partial molar entropy for the mixing of oxygen are given in Fig. 6. The former varied between −90 and −145 kJ mol^{-1} over the excess oxygen nonstoichiometry regime, which clearly demonstrated the effect of composition in preventing a zero excess partial molar enthalpy for the mixing of oxygen, as in an ideal solution. The latter also varied depending on the composition, further indicating that the excess entropy was not zero, unlike in a regular solution. Therefore, the activity coefficient should be considered in evaluating the thermodynamic quantities.

The standard enthalpy and entropy for the mixing of oxygen may further be calculated from the defect equilibrium with the metallic band conduction model by using the free electron gas approximation of Wagner [23]. The Fermi–Dirac distribution function was applied to define the chemical potential of quasi-electron species in metallic conductors because the concentration of the electronic carrier is not less than the density of state at the energy band [24, 25]. The electron density for two-dimensional electronic conductors is analytically solved

Fig. 5 Relationships between **a** $R/2\ln a_{\mathrm{O}_2}$ and $1/T$, and (**b**) $RT/2\ln a_{\mathrm{O}_2}$ and $1/T$

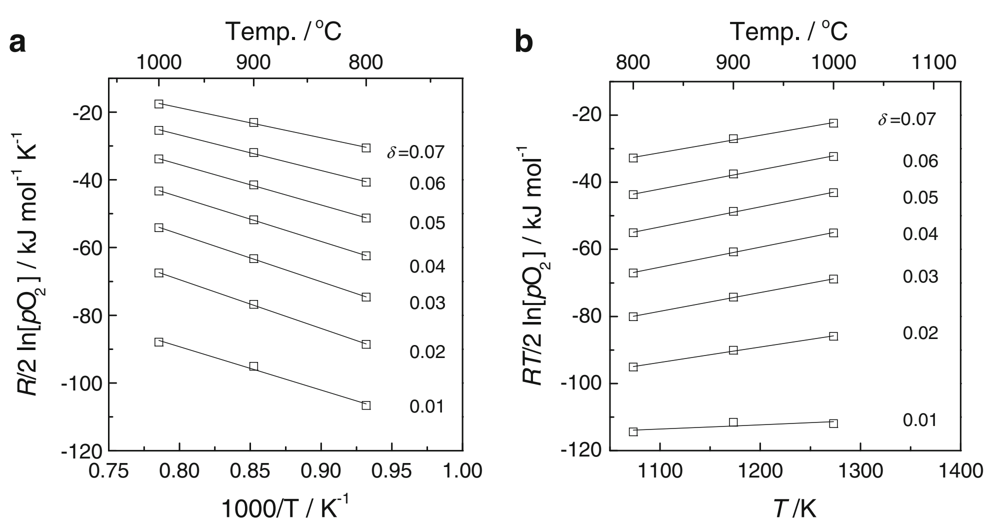

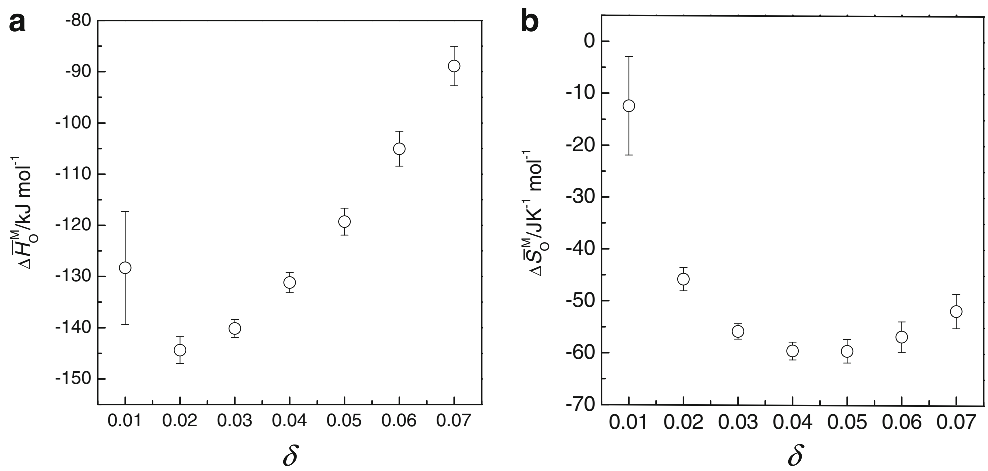

Fig. 6 **a** Partial molar enthalpy and **b** partial molar entropy for the mixing of oxygen for $La_2NiO_{4+\delta}$

and the relationship between the chemical potential of hole, $\mu_{h^\bullet}$, and the hole concentration, p, is expressed by [26]:

$$\mu_{h^\bullet} = \mu^o_{h^\bullet} + RT\ln\left\{\exp\left(\frac{N_A}{N_V V_m}[h^\bullet]\right) - 1\right\} \quad (8)$$

where $\mu^o_{h^\bullet}$, V_m, and N_V are the chemical potential of the hole in equilibrium with 1 bar oxygen, the molar volume of $La_2NiO_{4+\delta}$, and the density of state in the valence, respectively. The external and internal equilibriums are given by:

$$\frac{1}{2}O_2 + V_i^\times \rightleftharpoons O_i'' + 2h^\bullet \quad (9)$$

$$O_O^X + V_i^\times \overset{K_f}{\rightleftharpoons} O_i'' + V_O^{\bullet\bullet} \quad (10)$$

while keeping the electroneutrality as

$$p = 2[O_i''] = 2\beta\delta \quad (11)$$

where $V_i^\times$ represents the empty interstitial sites in the lattice, [ ] the concentration of the structure element therein ($p=[h^\bullet]$), and β the numerical conversion factor of concentration from "number of lattice molecule" to "number of unit volume" ($\beta=N_A/V_m$; N_A being the Avogadro number).

Since the chemical potential of each structure element k may be written in general as

$$\mu_k = \mu_k^o + RT\ln\frac{[k]}{N_k} + RT\ln\gamma_k \quad (12)$$

the reaction constant and Gibbs free energy change for reactions 9 and 10 may be written as [13]

$$\Delta G_O^o = -RT\ln\frac{[O_i'']}{a_{O_2}^{1/2}[V_i^\times]} - RT\ln\gamma_{O_i''} - 2RT\ln\left\{\exp\left(\frac{N_A}{N_V V_m}[h^\bullet]\right) - 1\right\} \quad (13)$$

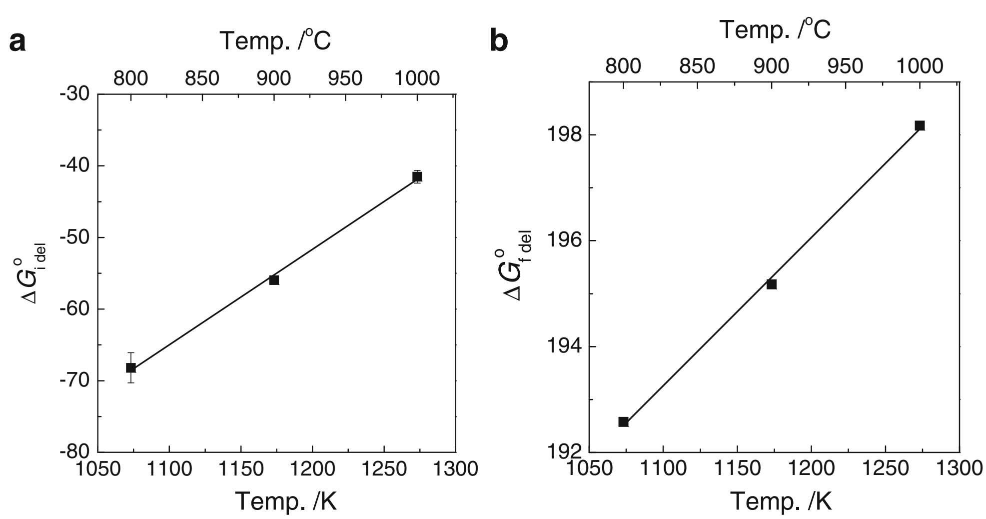

Fig. 7 Standard Gibbs free energy of **a** the mixing of oxygen and **b** of the Frenkel disorder for $La_2NiO_{4+\delta}$

Table 1 Values of the best fitting parameters to Eqs. 21a and 21b

Temperature (K)	$\Delta G_{\mathrm{I,del}}$ (kJ mol^{-1})	N_V (cm^{-3})	$\Delta G_{\mathrm{f,del}}$ (kJ mol^{-1})	b(× 10^5)	$\Delta H^{o}_{\mathrm{I,del}}$ (kJ mol^{-1})	$\Delta S^{o}_{\mathrm{I,del}}$ (J mol^{-1})
1,073	−68.19±2.10	2.51×10^{20}	192.57	5.73	−211±7	−133±6
1,173	−55.96±0.33	2.84×10^{20}	195.17	5.73	$\Delta H^{o}_{\mathrm{f,del}}$ (kJ mol^{-1})	$\Delta S^{o}_{\mathrm{f,del}}$ (J mol^{-1})
1,273	−41.52±0.89	3.30×10^{20}	198.17	5.73	162±1.4	−28±1

$$\Delta G^{o}_{\mathrm{f}} = -RT\ln\frac{[\mathrm{O}_i''][\mathrm{V}_O^{\bullet\bullet}]}{[\mathrm{O}_O^{\times}][\mathrm{V}_i^{\times}]} - RT\ln\frac{\gamma_{\mathrm{O}_i''}\gamma_{\mathrm{V}_O^{\bullet\bullet}}}{\gamma_{\mathrm{O}_O^{\times}}} \qquad (14-\mathrm{a})$$

$$K_{\mathrm{f}}^{\mathrm{del}} = \frac{[\mathrm{O}_i''][\mathrm{V}_O^{\bullet\bullet}]}{[\mathrm{O}_O^{\times}][\mathrm{V}_i^{\times}]}\frac{\gamma_{\mathrm{O}_i''}\gamma_{\mathrm{V}_O^{\bullet\bullet}}}{\gamma_{\mathrm{O}_O^{\times}}} \qquad (14-\mathrm{b})$$

A regular solution approximation is applied to the external reaction 9, and an ideal solution approximation is applied to the internal reaction 10.

$$\Delta H_{\mathrm{O}}^{xs} = -RT\ln\gamma_{\mathrm{O}_i''} = b\delta = b[\mathrm{O}_i''] \qquad (15)$$

where b is a constant representing the interactions among lattice ions and defects, which is independent of T and δ [27].

Site balances are given by the equation

$$[\mathrm{La}_{\mathrm{La}}^{\times}] = 2 \qquad (16)$$

$$[\mathrm{O}_O^{\times}] + [\mathrm{V}_O^{\bullet\bullet}] = 4 \qquad (17)$$

It has been reported that excess oxygen of $La_2NiO_{4+\delta}$ occupies the interstitial position in the LaO rock–salt layer having a relatively large free volume.

$$[\mathrm{O}_i''] + [\mathrm{V}_i^{\times}] = 2 \qquad (18)$$

The charge neutrality is given by

$$2[\mathrm{O}_i''] = [h] + 2[\mathrm{V}_O^{\bullet}] \qquad (19)$$

The degree of oxygen nonstoichiometry, δ, is given by

$$\delta = [\mathrm{O}_i''] - [\mathrm{V}_O^{\bullet\bullet}] \qquad (20)$$

From Eqs. 13–20, we obtain the relationship between δ and a_{O_2}

$$a_{O_2}^{1/2} = \frac{[\mathrm{O}_i'']}{(2-[\mathrm{O}_i''])}\exp\left[\frac{\Delta G^{o}_{\mathrm{O}} - b[\mathrm{O}_i'']}{RT} + 2\ln\left\{\exp\left(2\delta\frac{N_A}{N_V V_m}\right) - 1\right\}\right] \qquad (21a)$$

$$[\mathrm{O}_i''] = \frac{-(6K_f - \delta + K_f\delta) + \sqrt{(6K_f - \delta + K_f\delta)^2 + 8K_f(1-K_f)(4+\delta)}}{2(1-K_f^{\mathrm{del}})} \qquad (21b)$$

The solid lines in Fig. 4 are best fitted to Eqs. 21a and 21b with the fitting parameters, $\Delta G^{o}_{\mathrm{O}}$, $\Delta G^{o}_{\mathrm{F}}$, b, and N_V. The extracted standard partial molar Gibbs free energy for the mixing of oxygen and the formation Gibbs free energy of Frenkel disorder are shown in Fig. 7. The slope and intercept of the solid line in Fig. 7 yielded the standard partial molar enthalpy for the mixing of oxygen and entropy, $\Delta H^{o}_{\mathrm{O}}$ (−211±7 kJ mol^{-1}) and $\Delta S^{o}_{\mathrm{O}}$ (−133±6 Jmol^{-1}), respectively. Their numerical values are summarized in Table 1. The best fitted N_V values were around (2.5~3.3)×10^{20} eV^{-1} cm^{-3}, which is consistent with the literature data. The positive value of the formation Gibbs free energy of Frenkel disorder indicates the absence of any interstitial oxygen formation by intrinsic reaction in $La_2NiO_{4+\delta}$.

The partial thermodynamic quantities of $La_2NiO_{4+\delta}$ may also be interpreted by hole degeneracy using the Joyce–Dixon approximation of the Fermi–Dirac integral [28]. The effective density of states of the valence band is given by considering the internal degeneracy as [29]

$$N_V = 2\left(\frac{2\pi m_h^* kT}{h^2}\right)^{3/2} \qquad (22)$$

Table 2 Best estimates for the quantum concentration of the density of state in the valence (N_V) for the holes together with the evaluated ratio of the effective mass of holes to the rest mass, m_h^*/m_h

Temperature (K)	N_V (cm^{-3})	[12]	m_h*/m_o	[12]
1,073	2.47×10^{20}	2.24×10^{20}	1.28±0.15	1.20±0.05
1,173	2.79×10^{20}	2.75×10^{20}	1.27±0.06	1.27±0.10
1,273	3.21×10^{20}	3.24×10^{20}	1.29±0.04	1.30±0.08

Table 3 The oxidation reaction equilibrium constant K_{ox} together with the standard reaction free energy, as evaluated, and compared with literature values

Temperature (K)	K_{ox}	ΔG^{o}_{ox} (kJ)			
		This work	[12]	[10]	[13]
1,073	2,740±2.32	−71±0.01	−52	−5	−88
1,173	534±1.39	−61±0.03	−36	8	−87
1,273	142±1.19	−52±0.09	−24	22	−86

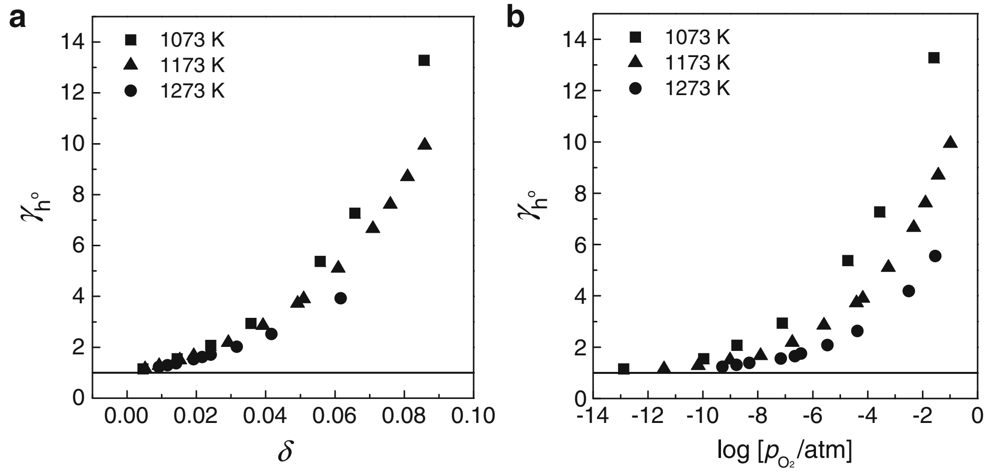

Fig. 8 Activity coefficient of holes vs. nonstoichiometry (**a**) and oxygen activity (**b**) at different temperatures for $La_2NiO_{4+\delta}$

where m_h^* denotes the effective mass of holes. The equilibrium constant for the external reaction, Eq. 9, may be written as

$$K_{ox} \equiv \exp\left(-\frac{\Delta G_O^o}{RT}\right) = \frac{\left(\gamma^{\times}_{O''_i}\frac{[O''_i]}{N_i}\right)\left(\gamma_{h^\bullet}\frac{p}{N_V}\right)^2}{p_{O_2}^{1/2}\gamma_i^{\times}\frac{[V_i^{\times}]}{N_i}} \tag{23}$$

The activity coefficients, γ, become proportional to an increasing positive power of the concentration, especially when $k/N_k \geq 0.1$, where k is the defect species and N_k the density of state of species k. For particles of atomic mass, the density of states exceeds 10^{24} cm^{-3} at ordinary temperatures (in case of $La_2NiO_{4+\delta}$, $N_i \approx 10^{22}$ cm^{-3} around 1,073 K [17]), which is many orders of magnitude larger than that for particles with free electron mass and thus larger than the maximum accessible concentration for atomic particles. Therefore, the much faster increase in $\mu_{h^\bullet}$ with increasing oxygen excess may be ascribed to the positive deviation of the activity coefficient of the hole. One may expect $\gamma_{O''_i} \approx 1 \approx \gamma_{V_O^{\times}}$, but $\gamma_{h^\bullet} > 1$ in Eq. 23, as consistent with the Gibbs–Helmholtz equation for a regular solution.

The activity coefficient of holes has been described from Eq. 12 as [30]

$$\frac{\gamma_{h^\bullet} p}{N_V} = \exp\left(\frac{\mu_{h^\bullet} - \mu_{h^\bullet}^o}{RT}\right) = \exp\eta\ ; \eta \equiv -\frac{E_F - E_V}{kT} \tag{24}$$

where E_F and E_V are the Fermi energy and the energy at the upper edge of the valence band, respectively. The activity coefficient of holes due to the Joyce–Dixon approximation can be obtained with the Fermi–Dirac integral [28, 29]

$$\ln\gamma_{h^\bullet} = \eta - \ln\frac{p}{N_V} = \frac{1}{\sqrt{8}}\frac{p}{N_V} + \left(\frac{3}{16} - \frac{\sqrt{3}}{9}\right)\left(\frac{p}{N_V}\right)^2 + \cdots \tag{25}$$

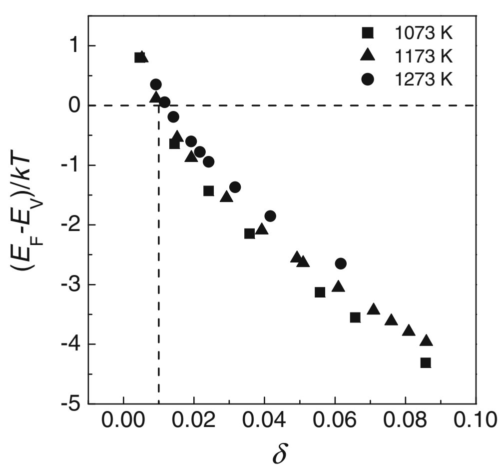

Fig. 9 Fermi energy relative to the valence band edge vs. oxygen excess of $La_2NiO_{4+\delta}$ at different temperatures

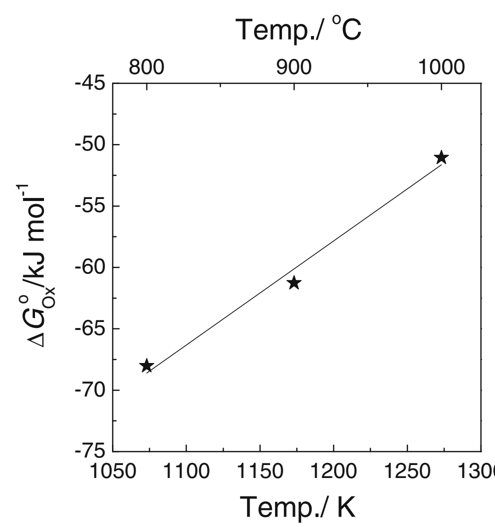

Fig. 10 Standard reaction free energy of oxygen vs. temperature of $La_2NiO_{4+\delta}$

Table 4 Values of the best estimates of standard partial molar enthalpy and entropy for the mixing of oxygen for $La_2NiO_{4+\delta}$

	This work	[12]	[10]	[13]
$\Delta H^{\mathrm{o}}_{\mathrm{ox}}$, kJ	−152	−199	−150	−213
$\Delta S^{\mathrm{o}}_{\mathrm{ox}}$, J	−79	−138	−135	−126

By substituting Eq. 25 into Eq. 23 with the second-order term approximation, the modified isotherm relationship between nonstoichiometry and a_{O_2} can be obtained as

$$2\left[\frac{1}{\sqrt{8}}\frac{2\beta\delta}{N_{\mathrm{V}}}+\left(\frac{3}{16}-\frac{\sqrt{3}}{9}\right)\left(\frac{2\beta\delta}{N_{\mathrm{V}}}\right)^2\right]+\ln\frac{\delta}{2-\delta}\left(\frac{2\beta\delta}{N_{\mathrm{V}}}\right)^2=\ln K_{\mathrm{ox}}+\frac{1}{2}\ln a_{O_2} \tag{26}$$

The broken solid lines in Fig. 4 are the best fitted to Eq. 26 with the fitting parameters, K_{ox} and N_{V}, with χ^2 values (0.01–0.31 depending on temperatures) as a measure of fitting accuracy. The best-estimated values are listed in Tables 2 and 3, respectively.

The density of states of the valence band varied from 2.5×10^{20} to 3.2×10^{20} cm^{-3} depending on temperature, which is in excellent agreement with the values calculated from the Gibbs–Helmholtz equation for the regular solution. From Eq. 22, the effective mass of holes, m_{h}^*, may by calculated to be 1.27–1.29 times the rest mass, m_{h}, which indicates the action of band-like conduction and allows the effect of the small degree of polaron hopping to be ignoring. Now, from the Eq. 25, the activity coefficient of holes may be calculated against the oxygen nonstoichiometry or oxygen activity. Figure 8 clearly illustrates the early positive deviation of the activity coefficient of holes from unit, leading to $\gamma_{\mathrm{h}^\bullet}\approx14$ at $\delta\approx0.08$ which is quite close to the literature values ($\gamma_{\mathrm{h}^\bullet}\approx10$ at $\delta\approx0.08$).

The Fermi energy was also successfully calculated from Eq. 24, relative to the upper edge of the valence band against an oxygen nonstoichiometry. As shown in Fig. 9, the Fermi energy was already submerged below the valence band edge with an oxygen excess nonstoichiometry of $\delta\approx0.01$, suggesting the strong possibility of band conduction.

Figure 10 shows the standard reaction free energy of the reaction in Eq. 9 vs. temperature, and the results were best fitted as

$$\Delta G^{\mathrm{o}}_{\mathrm{ox}}=-(160\pm11)+(85\pm9)\times10^{-3}T \tag{27}$$

in the temperature range investigated. From the slope and intercept of the solid line in Fig. 10, the standard reaction enthalpy and entropy of reaction Eq. 9 were calculated, as listed in Table 4, and found to be in reasonable agreement with the values calculated by the Gibbs–Helmholtz equation.

The partial molar enthalpy and the partial molar entropy for the mixing of oxygen can be calculated from Eq. 26 using Eq. 5, respectively, as [15]

$$\Delta\overline{H}^{\mathrm{M}}_{\mathrm{O}}=\left(\frac{\partial(\Delta\overline{G}^{\mathrm{M}}_{\mathrm{O}}/T)}{\partial(1/T)}\right)_\delta=\Delta H^{\mathrm{o}}_{\mathrm{ox}}+3RT+6RT\left[\frac{1}{2\sqrt{8}}\frac{2\beta\delta}{N_{\mathrm{V}}}+\left(\frac{3}{16}-\frac{\sqrt{3}}{9}\right)\left(\frac{2\beta\delta}{N_{\mathrm{V}}}\right)^2\right] \tag{29}$$

$$\Delta\overline{S}^{\mathrm{M}}_{\mathrm{O}}=-\left(\frac{\partial\,\Delta\overline{G}^{\mathrm{M}}_{\mathrm{O}}}{\partial T}\right)_\delta=\Delta S^{\mathrm{o}}_{\mathrm{ox}}-R\ln\frac{\delta}{2-\delta}\left(\frac{2\beta\delta}{N_{\mathrm{V}}}\right)^2+3R+R\left[\frac{1}{\sqrt{8}}\frac{2\beta\delta}{N_{\mathrm{V}}}+4\left(\frac{3}{16}-\frac{\sqrt{3}}{9}\right)\left(\frac{2\beta\delta}{N_{\mathrm{V}}}\right)^2\right] \tag{30}$$

From Eqs. 29 and 30, the excess partial molar enthalpy and entropy for the mixing of oxygen were

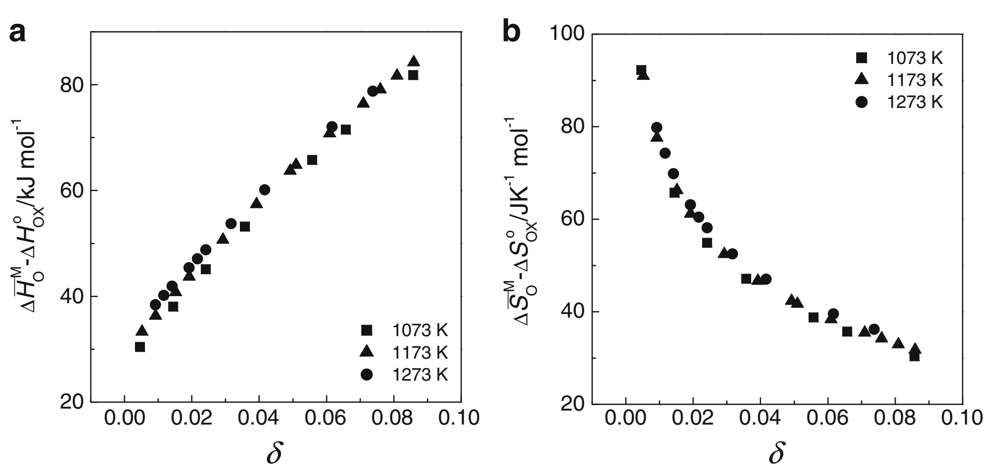

Fig. 11 Relative partial molar enthalpy (**a**) and entropy (**b**) for the mixing of oxygen against oxygen nonstoichiometry

calculated and are represented in Fig. 11 as a function of the oxygen nonstoichiometry δ. The positive values of $\Delta H_{\mathrm{O}}^{\mathrm{xs}}\left(=\Delta\overline{H}_{\mathrm{O}}^{\mathrm{M}}-\Delta H_{\mathrm{O}}^{\mathrm{o}}\right)$ from $3RT$ to 90 kJ mol^{-1} as δ was increased from 0 to 0.09 supported the positive deviation of system and appear to be in good agreement with literature data.

Conclusion

The oxygen excess nonstoichiometry of $La_2NiO_{4+\delta}$ was measured as a function of temperature and pO_2 by coulometric titration method. A positive deviation from the ideal dilution solution behavior was exhibited, and the partial molar thermodynamic quantities of $La_2NiO_{4+\delta}$ were calculated from the Gibbs–Helmholtz equation for regular solution by introducing the activity coefficient of the charge carriers. The activity coefficient of holes was successfully calculated by using the Joyce–Dixon approximation of the Fermi–Dirac integral.

The effective mass of holes, m_h^*, was 1.27–1.29 times the rest mass, m_h, which indicated the action of band-like conduction and allowed the effect of the small degree of polaron hopping to be ignored. The activity coefficient of holes calculated against the oxygen nonstoichiometry clearly illustrated the early positive deviation of the activity coefficient of holes from unity, leading to $\gamma_{h^\bullet}\approx 14$ at $\delta\approx 0.08$, which is quite close to the literature value of $\gamma_{h^\bullet}\approx 10$ at $\delta\approx 0.08$. All the evaluated thermodynamic quantities were in good agreement with the experimental literature values.

Acknowledgments This research was supported by Basic Science Research Program through the National Research Foundation of Korea funded by the Ministry of Education, Science and Technology (2009-0090172).

References

1. Mauvy F, Lalanne C, Bassat JM, Grenier JC, Zhao H, Dordor P, Stevens Ph (2005) J Eur Ceram Soc 25:2669–2672
2. Smith JB, Norby T (2006) J Electrochem Soc 153:A233–A238
3. Ishihara T, Miyoshi S, Furuno T, Sanguanruang O, Matsumoto H (2006) Solid State Ionics 177:3087–3091
4. Kharton VV, Kovalevsky AV, Avdeev M, Tsipis EV, Patrakeev MV, Yaremchenko AA, Naumovich EN, Frade JR (2007) Chem Mater 19:2027–2033
5. Naumovich EN, Patrakeev MV, Kharton VV, Yaremchenko AA, Logvinovich DI, Marques FMB (1999) Solid State Ionics 119:23–30
6. Patrakeev MV, Naumovich EN, Kharton VV, Yaremchenko AA, Tsipis EV, Núñez P, Frade JR (2005) Solid State Ionics 176:179–188
7. Kilner JA, Shaw CKM (2002) Solid State Ionics 154–155:523–527
8. Jorgensen JD, Dabrowski B, Pei S, Richards DR, Hinks DG (1989) Phys Rev B 40:2187–2199
9. Bassat JM, Odier P, Villesuzanne A, Marin C, Pouchard M (2004) Solid State Ionics 167:341–347
10. Naumovich EN, Kharton VV (2010) J Mol Struct Theochem 946:57–64
11. Chroneos A, Parfitt D, Kilner JA, Grimes RW (2010) J Mater Chem 20:266–270
12. Parfitt D, Chroneos A, Kilner JA, Grimes RW (2010) Phys Chem Chem Phys 12:6834–6836
13. Nakamura T, Yashiro K, Sato K, Mizusaki J (2009) Solid State Ionics 180:368–376
14. Tsipis EV, Naumovich EN, Patrakeev MV, Waerenborgh JC, Pivak YV, Gaczynski P, Kharton VV (2007) J Phys Chem Solids 68:1443–1455
15. Kim H-S, Yoo H-I (2010) Phys Chem Chem Phys 12:4704–4713
16. Nakamura T, Yashiro K, Sato K, Mizusaki J (2009) Phys Chem Chem Phys 11:3055–3062
17. Nakamura T, Yashiro K, Sato K, Mizusaki J (2009) J Solid State Chem 182:1121–1128
18. Boehm E, Bassat JM, Dordor P, Mauvy F, Grenier JC, Stevens Ph (2005) Solid State Ionics 176:2717–2725
19. Millburn JE, Green MA, Neumann DA, Rosseinsky MJ (1999) J Solid State Chem 145:401–420
20. Kang S-H, Yoo H-I (1996) Solid State Ionics 86–88:751–755
21. Lee D-K, Jeon J-I, Kim M-H, Choi W, Yoo H-I (2005) J Solid State Chem 178:185–193
22. Naumovich EN, Patrakeev MV, Kharton VV, Yaremchenko AA, Longvinovich DI, Marques FMB (2005) Solid State Sci 7:1353–1362
23. Wagner C (1953) J Chem Phys 21:1819–1827
24. Kröger FA (1974) The chemistry of imperfect crystals, vol 2, 2 revisedth edn. North Holland, The Netherlands, Chap 7 and 9
25. Lankhorst MHR, Bouwmeester HJM, Verweji H (1997) J Solid State Chem 133:555–567
26. Hook JR, Hall HE (1991) Solid state physics, 2nd edn. Wiley, England, pp 399–415
27. Mizusaki J, Yamauchi S, Fueki K, Ishikawa A (1984) Solid State Ionics 12:119–124
28. Joyce WB, Dixon RW (1997) Appl Phys Lett 31(5):354–356
29. Kittel C, Kroemer H (1980) Thermal physics, 2nd edn. Freeman and Company, New York, Chap 133
30. Rosenberg AJ (1960) J Chem Phys 33(3):665–667